Free Radical Biology and Medicine 178 (2022) 295–307

Contents lists available at ScienceDirect

Free Radical Biology and Medicine

journal homepage: www.elsevier.com/locate/freeradbiomed

Central nervous system and systemic oxidative stress interplay with inflammation in a bile duct ligation rat model of type C hepatic encephalopathy

K. Pierzchala [a,b,c,*], D. Simicic [a,b,c], A. Sienkiewicz [d,e], D. Sessa [f], S. Mitrea [a,b], O. Braissant [g], V. A. McLin [f], R. Gruetter [a,c], C. Cudalbu [a,b]

[a] Center for Biomedical Imaging, EPFL, Lausanne, Switzerland
[b] Animal Imaging and Technology, Ecole Polytechnique Fédérale de Lausanne, Lausanne, Switzerland
[c] Laboratory of Functional and Metabolic Imaging, EPFL, Lausanne, Switzerland
[d] Laboratory for Quantum Magnetism, Institute of Physics, EPFL, Lausanne, Switzerland
[e] ADSresonances Sàrl, Préverenges, Switzerland
[f] Swiss Pediatric Liver Center, Department of Pediatrics, Gynecology and Obstetrics, University Hospitals Geneva and University of Geneva, Geneva, Switzerland
[g] Service of Clinical Chemistry, Lausanne University Hospital and University of Lausanne, Lausanne, Switzerland

ARTICLE INFO

Keywords:
Hepatic encephalopathy
Central nervous system
CNS and Systemic oxidative stress
Antioxidants
Inflammation

ABSTRACT

The role and coexistence of oxidative stress (OS) and inflammation in type C hepatic encephalopathy (C HE) is a subject of intense debate. Under normal conditions the physiological levels of intracellular reactive oxygen species are controlled by the counteracting antioxidant response to maintain redox homeostasis. Our previous *in-vivo* ^{1}H-MRS studies revealed the longitudinal impairment of the antioxidant system (ascorbate) in a bile-duct ligation (BDL) rat model of type C HE.

Therefore, the aim of this work was to examine the course of central nervous system (CNS) OS and systemic OS, as well as to check for their co-existence with inflammation in the BDL rat model of type C HE. To this end, we implemented a multidisciplinary approach, including *ex-vivo* and *in-vitro* electron paramagnetic resonance spectroscopy (EPR) spin-trapping, which was combined with UV–Vis spectroscopy, and histological assessments. We hypothesized that OS and inflammation act synergistically in the pathophysiology of type C HE.

Our findings point to an increased CNS- and systemic-OS and inflammation over the course of type C HE progression. In particular, an increase in the CNS OS was observed as early as 2-weeks post-BDL, while the systemic OS became significant at week 6 post-BDL. The CNS EPR measurements were further validated by a substantial accumulation of 8-Oxo-2′-deoxyguanosine (Oxo-8-dG), a marker of oxidative DNA/RNA modifications on immunohistochemistry (IHC). Using IHC, we also detected increased synthesis of antioxidants, glutathione peroxidase 1 (GPX-1) and superoxide dismutases (*i.e.*Cu/ZnSOD (SOD1) and MnSOD (SOD2)), along with proinflammatory cytokine interleukin-6 (IL-6) in the brains of BDL rats. The presence of systemic inflammation was observed already at 2-weeks post-surgery. Thus, these results suggest that CNS OS is an early event in type C HE rat model, which seems to precede systemic OS. Finally, our results suggest that the increase in CNS OS is due to enhanced formation of intra- and extra-cellular ROS rather than due to reduced antioxidant capacity, and that OS in parallel with inflammation plays a significant role in type C HE.

1. Introduction

Of all the organs, the central nervous system (CNS) has the most intensive oxidative metabolism [1]. Under normal physiological conditions reactive oxygen and nitrogen species (ROS and RNS) play an important role in signal transduction cascades. They are also acknowledged for their role as crucial mediators of immune defense [2–4]. However, a permanent increase in ROS and RNS levels is harmful on cell- and tissue-homeostasis because it results in oxidative stress (OS).

In the context of OS, it is worth mentioning that OS and inflammation are strongly linked and interdependent pathophysiological

* Corresponding author. Center for Biomedical Imaging, EPFL, Lausanne, Switzerland.
E-mail address: katarzyna.pierzchala@epfl.ch (K. Pierzchala).

https://doi.org/10.1016/j.freeradbiomed.2021.12.011
Received 30 September 2021; Received in revised form 12 November 2021; Accepted 6 December 2021
Available online 8 December 2021

Abbreviations

ALT/GPT	alanine aminotransferase
Asc	ascorbate
AST/GOT	aspartate aminotransferase
BBB	blood-brain barrier
BDL	bile-duct ligation
C HE	type C hepatic encephalopathy
CLD	chronic liver disease
CMH	1-hydroxy-3-methoxycarbonyl-2,2,5,5-tetramethyl pyrrolidine hydrochloride
CNS	central nervous system
EPR	electron paramagnetic resonance spectroscopy
Gln	glutamine
GPX-1	glutathione peroxidase 1
GSH	glutathione
$HO^{\cdot}$	- hydroxyl radical
IF	immunofluorescence
IHC	immunohistochemistry
IL-6	interleukin-6
LTD	long-term depression
LTP	long-term potentiation
LYM	Lymphocytes
MFI	mean fluorescence intensity
NBT	Nitroblue Tetrazolium
OS	oxidative stress
$O_2^{\cdot-}$	- superoxide anion
Oxo-8-dG	8-Oxo-2′-deoxyguanosine
PMA	phorbol-12-myristate-13-acetate
PMN	polymorphonuclear neutrophils
ROS/RNS	reactive oxygen and nitrogen species
RT	room temperature
SOD	superoxide dismutase
WBC	white blood cells

processes [5]. In fact, it is widely accepted that in the presence of OS, inflammatory processes will develop, thus further promoting the progression of OS. Similarly, in the event that inflammation is the trigger, an OS response will be promoted and will contribute to the inflammatory response [4,6]. Therefore, OS is considered to be related to innate inflammation and seems to be a common thread among many neurodegenerative disorders associated with cognitive deficits [7–11].

Under physiological conditions ROS are critical for hippocampal synaptic plasticity (learning and memory, including long-term potentiation (LTP)), but when in excess, ROS become neurotoxic leading to neurodegeneration, aging/disease-related impairment, and long-term depression (LTD) [12,13]. Among ROS, the superoxide anion ($O_2^{\cdot-}$) is of critical importance for biological systems. Specifically, $O_2^{\cdot-}$, the primary ROS generated through the mitochondrial energy production pathway, is involved in many cellular processes of physiological significance, including cell signaling. However, when in excess, $O_2^{\cdot-}$ becomes deleterious to cellular structure and function: reduction of $O_2^{\cdot-}$ leads to other, more reactive forms of ROS, such as the highly reactive hydroxyl radical ($HO^{\cdot}$). It is widely accepted that ROS are short-lived, as they react rapidly with first line antioxidants, that is low-molecular weight reductants, like glutathione (GSH) or ascorbate (Asc) [14,15]. Thus, in living cells, antioxidants maintain the redox homeostasis and keep the balance between ROS generation and elimination [16].

Type C hepatic encephalopathy (C HE), a severe neuropsychiatric disorder, arises in the setting of liver dysfunction, which is unable to remove toxins from the blood, including ammonia. This, in turn, results in elevated plasma levels of ammonium cations (NH_4^+) and a resultant accumulation of glutamine (Gln) in the brain [8,17]. It is becoming increasingly evident that the development and acceleration of type C HE is a multifactorial process with OS and inflammation being important players in addition to the osmotic effect of Gln [18,19]. Factors involved in the precipitation of HE episodes such as ammonia, hyponatremia and inflammatory cytokines have been shown to trigger a self-amplifying cycle between astrocyte osmotic stress and cerebral oxidative/nitrosative stress [20]. The presence of systemic OS has been shown in BDL rat [21]. In addition, an indirect detection of ROS in brain homogenates, using biochemical markers, unveiled a correlation between experimental obstructive jaundice and OS at 5- and 10-days post-BDL [22]. Studies carried on *post-mortem* brain tissue of cirrhotic and HE patients have indicated that OS is a hallmark of HE but not of cirrhosis itself [23]. However, direct evidence and impact of CNS- and systemic- OS on HE progression is limited.

Circulating and brain cytokines together with endotoxins (*i.e.,* NH_4^+) can generate an inflammatory cascade that will exacerbate OS [18,20,24,25]. There is also evidence in support of a synergistic interaction between NH_4^+, ROS, RNS and inflammatory cytokines in astrocyte osmotic stress/brain edema. White blood cells (WBC), and especially polymorphonuclear neutrophils (PMN) participate in immune and inflammatory processes by releasing large amounts of pro-inflammatory cytokines and ROS/oxidative burst. When in excess, these cause endothelial dysfunction and increase the leakiness of the blood vessels/blood-brain barrier (BBB) [2,3,9,26,27]. Clinically, it has been shown that systemic inflammation is associated with neuroinflammation and contributes to acute worsening of patients with type C HE. Moreover, it is believed that both OS and astrocytes and microglia activation are implicated in the pathogenesis of type C HE [28,29]. Specifically, microglia activation causes an increase in OS and secretion of matrix metalloproteinases, which can lead to neuronal damage and increased BBB permeability [30]. Studies have demonstrated that severe PMN dysfunction was linked to cirrhosis, increasing the risk of infection, organ failure, and mortality in patients with cirrhosis [31]. In contrast to acute HE, evidence for neuroinflammation in type C HE is still incomplete.

In biological systems, *in-vivo* steady-state concentrations of ROS exist in the pico-to nanomolar range [2], and their lifetimes span nanoseconds to seconds (*e.g.* $O_2^{\cdot-}$ lifetime is suggested to be in the μs regime), depending on local antioxidants concentrations and clearance mechanisms [14]. Naturally, this makes their direct *in-vivo* detection difficult [15]. Therefore, biological systems require probes for OS detection that can rapidly react with ROS to compete with antioxidants and create a stable radical, which then can be quantified. Most experimental assays to quantify ROS levels in biological systems provide relative data, which are usually expressed in arbitrary units (a.u.). To this end, electron paramagnetic resonance (EPR) in combination with spin-trapping is a unique analytical technique, which allows for direct and reliable detection of the ROS presence in the system under study. This approach is also less uncertain as compared to other methods (*i.e.*: immunoassays or UV–Vis spectroscopy). Thus, EPR spin-trapping provides useful information concerning tissue/blood redox state and offers significant advantages over the other approaches. Moreover, being a technique yielding quantitative data, this approach shows a very strong potential for future clinic applications. In the present study, we used the advantages of the EPR spin-trapping technique, a cyclic hydroxylamine 1-hydroxy-3-methoxycarbonyl-2,2,5,5-tetramethyl pyrrolidine hydrochloride (CMH) spin-trap readily reacted with cytoplasmic and mitochondrial $O_2^{\cdot-}$ and generated stable nitroxide radicals, thus allowing for quantitative data analysis [7,32,33].

Our previous *in-vivo* ^{1}H-MRS studies have revealed the longitudinal decrease of brain antioxidant Asc together with the increase in plasma NH_4^+ and brain Gln in BDL rats [29]. Therefore, we aimed to advance our

understanding of type C HE by analyzing for the first time the time course of CNS OS and systemic OS synchronously with markers of systemic and local inflammation by using a multimodal approach which combines *ex-vivo* and *in-vitro* EPR spectroscopy with UV–Vis spectroscopy and histological assessments of the brains of BDL rats.

2. Materials and methods

2.1. BDL rat model of CLD

All experiments were approved by the Committee on Animal Experimentation for the Canton de Vaud, Switzerland (VD3022/VD2439). Wistar male adult rats (n = 51, 125–150 g, Charles River Laboratories, L'Arbresle, France) were used: 30 rats underwent BDL as previously described [34] while 21 were SHAM operated. The exact number of rats per measurement is provided below for each corresponding experiment. Animals had unlimited access to standard rat chow and water for the duration of study. The BDL rat model is validated by the ISHEN commission as a model reflecting HE associated with cirrhosis, portal hypertension and hyperammonemia [35].

2.2. Biochemical measurements

Blood samples were taken from the sublingual vein (1 mL) before BDL (n = 13) and SHAM (n = 4) surgery and at post-surgery weeks 2 (BDL: n = 20, SHAM n = 7), 4 (BDL: n = 18, SHAM n = 7), 6 (BDL: n = 16, SHAM n = 5) and 8 (BDL n = 4, SHAM n = 2). Liver parameters (plasma bilirubin, aspartate aminotransferase (AST/GOT) and Alanine Aminotransferase (ALT/GPT)) and glucose were measured using a Reflotron® Plus system (F. Hoffmann-La Roche Ltd). Blood NH_4^+ was measured with a blood ammonia meter (PocketChemTM BA PA-4140).

2.3. Electron paramagnetic resonance spectroscopy (EPR) for CNS and systemic OS measurements

2.3.1. Brain tissue preparation

Two EPR studies were performed. We have first measured the OS in cerebellum and hippocampus at 6-weeks post-BDL (BDL: n = 3 and SHAM: n = 3). Then a longitudinal study was performed only in the hippocampus at week 2 (BDL n = 2, SHAM n = 2), 4 (BDL n = 2, SHAM n = 2), 6 (total: BDL n = 5, SHAM n = 5) and 8 post-BDL (BDL n = 2, SHAM n = 2) to identify early changes in OS.

Rats were pre-anesthetized with 4% isoflurane (Piramal Enterprises Ltd.) for 5 min followed by subcutaneous injection of the analgesic (Temgesic (ESSEX), 0.03 mg/mL in 0.9% NaCl). 15 min later an intracardiac perfusion was performed via the left ventricle with cell culture medium RPMI-1640 (pH 7.4, R8758 Sigma) supplemented with 10% of Fetal Bovine Serum (FBS, F2442 Sigma) and 1% of antibiotics (P4083 Sigma), and vena cava dissection to wash out blood and keep the brain cells alive. Finally, brain extraction was completed. To preserve cell viability after extraction, the cerebellum and hippocampi (right and left) were weighed and immediately transferred into a 5 mL Eppendorf tube with whole RPMI-1640 medium immersed in ice. Afterwards, tissue was sliced into small pieces, transferred into a 2 mL syringe with whole RPMI-1640 medium and 10 mM CMH cell-permeable spin-trap (Noxygen Science Transfer & Diagnostics GmbH) and incubated at 37 °C. After each incubation time (1 h of incubation with 6 timepoints) ~50 μL of cell suspensions were transferred into 1.5 mm ID and 1.8 mm OD quartz capillary tubes (VitroCom, USA, sample height of 25 mm) and sealed with Leica Critoseal™ (Leica Microsystems GmbH) for further EPR measurements.

2.3.2. Blood sample preparation

Blood samples were withdrawn from the sublingual vein (1 mL) before BDL or SHAM surgery and post-surgery at weeks 2, 4, 6 and 8 (BDL n = 4, SHAM n = 2, per time point). 1 mL of blood was collected into sterile tube pretreated with EDTA (ED2P Sigma, 1.5 mg/mL) and mixed with CMH spin-trap. The final CMH concentration was 10 mM. Prior to EPR measurements, the blood samples were incubated for 1 h, during which, at equal time intervals, six aliquots of ~7 μL were collected and transferred into 0.7 mm ID and 0.87 mm OD quartz capillary tubes (VitroCom, USA, sample height of 25 mm) and sealed with Leica Critoseal™ (Leica Microsystems GmbH).

2.3.3. EPR measurements

EPR spectra were collected at room temperature (RT) using an X-band EPR spectrometer, Model ESP300E (Bruker-BioSpin, Karlsruhe, Germany) equipped with a standard rectangular TE_{102} cavity. For each experimental time point of ROS detection with CMH, two-scan field-swept EPR spectra were recorded. The setting for brain tissue and systemic OS detection were: microwave frequency ~9.78 GHz, microwave power 2 mW, sweep width 100 G, modulation frequency 100 kHz, modulation amplitude 0.5 G, receiver gain 5×10^3, time constant 40.9 ms, conversion time 81 ms.

Spectra were evaluated and processed by OriginPro (OriginLab, USA). The double-integration of EPR spectra yielded the total EPR signal intensities of the oxidized (paramagnetic) form of the CMH spin-trap. The ROS generation rates were calculated from the kinetic plots of generated CMH radicals. The intracellular concentrations of CMH were converted into an absolute value (μmol/g/min or μmol/μL/min) using TEMPOL radical as external standard. ROS generation rates were calculated from EPR kinetic plots (EPR signal levels versus the elapsed time), normalized to the tissue weight and averaged.

2.4. Nitroblue tetrazolium (NBT) staining – histo-enzymatic technique for ROS visualization

NBT (N5514 Sigma, 1.6 mg/mL) in HBSS (H9269 Sigma) and filtered with a 0.22 μm filter (SLGS033SS Millipore) was applied to detect the extra and intracellular ROS/superoxide anion $(O_2^{\cdot-})$ generation. By reacting with cellular $O_2^{\cdot-}$, NBT indirectly reflects the redox activity of living cells. The reduction product, a dark blue precipitate of formazan, can be monitored by microscopy and UV–Vis spectroscopy [27,36,37].

2.4.1. CNS oxidative stress using microscopic NBT assay

The extracted hippocampus and cerebellum (BDL week 8 n = 3, SHAM week 8 n = 3) were incubated in the dark with fresh NBT at 37 °C in 5% CO_2 for 0.5 h for histochemical detection of OS and then imaged using a stereomicroscope (MEIJI-TECHNO CO., EMZ-13TR).

2.4.2. Systemic oxidative stress using microscopic NBT assay

Lymphocytes (LYM) and Polymorphonuclear (PMN) cells isolation: Rats were pre-anesthetized with 4% isoflurane (Piramal Enterprises Ltd.) for 5 min and subcutaneous injection of the analgesic (Temgesic (ESSEX), 0.03 mg/mL in 0.9% NaCl) was performed 15 min before blood withdrawal. Sterile blood samples were obtained from the heart (terminal procedure) of BDL and SHAM rats at week 8 (n = 3 per group). Blood was collected into sterile syringes pretreated with EDTA (ED2P Sigma, 1.5 mg/mL). For each isolation procedure, the same volume of anti-coagulated blood was used (7 mL) to ensure proper comparison. The dextran sedimentation was applied for red blood cells (RBC) removal and then leukocytes were separated by centrifugation on a Ficoll (GE17-1440-02 Sigma) layer. The remaining RBC were lysed by hypotonic shock.

LYM and PMN were then resuspended in RPMI-1640 whole medium and allowed to adhere to Eppendorf Cell Imaging Coverglass (sterile 2 chambers, 0030742010 Eppendorf AG) for 1 h at 37 °C in 5% CO_2. The adhered cells were treated for 1 h with 150 μL of NBT (basic) or NBT supplemented with phorbol-12-myristate-13-acetate at 400 ng/mL (PMA – phagocytic cells stimulation/cytoplasmic $O_2^{\cdot-}$ stimulation with

nicotinamide adenine dinucleotide phosphate (NADPH) oxidases activator)(3 replicates per cells group per rat and test type (NBT, NBT + PMA)) to detect $O_2^{\cdot-}$. The stimulation assay mimics physiological *in-vivo* activation and is performed to test for a transient decrease of responsiveness. After incubation cells were washed twice with phosphate buffered saline (PBS, P5493 Sigma), air dried and methanol fixed. Safranin-O solution 1% (84120 Sigma) was applied to stain cell nuclei. The percentage of formazan-positive cells was evaluated (NBT test: BDL PMN ~ 600 cells, BDL LYM ~ 800 cells, SHAM PMN ~ 200 cells, SHAM LYM ~ 200 cells; NBT + PMA test: BDL PMN ~ 200 cells, BDL LYM ~ 2400 cells, SHAM PMN ~ 100 cells, SHAM LYM ~ 500 cells). LYM and PMN were scored as: no detectable formazan (−), scattered formazan granules (+), intermediate density (++), and cells filled with formazan (+++) [37,38].

2.4.3. Systemic oxidative stress UV–Vis spectroscopy using colorimetric NBT assay

LYM and PMN isolated cells were seeded in 24-well culture plates to determine $O_2^{\cdot-}$ production after reaction with NBT. Both NBT and NBT + PMA tests were repeated. After 1 h cells were washed twice with PBS, followed by methanol wash, and then air dried. The intracellular formazan precipitants were dissolved by adding 120 μL of 2 M KOH for membrane solubilization followed by 140 μL of DMSO and then shaken for 10 min at RT. 100 μL of solution were transferred into 96-well plate, and the absorbance was measured at 540 nm (Hidex Sense Beta, Hidex Oy).

2.5. Systemic inflammation

2.5.1. Blood smears

Giemsa staining on peripheral blood smears was performed to visualize the LYM and PMN count and to examine cellular morphology [39]. Blood samples were withdrawn from the sublingual vein (100 μL) at week 0 before BDL and SHAM surgery (n = 4 per group) and the post-surgery weeks 2 (n = 8 and n = 6 per group), 4 (n = 6 per group), 6 (n = 4 per group) and 8 (n = 3 per group), respectively.

2.5.2. Lymphocytes and polymorphonuclear cells isolation and concentration assay

LYM and PMN were isolated from blood of BDL and SHAM rats as described above at weeks 2 (n = 2, n = 2), 4 (n = 2, n = 2), 6 (n = 4, n = 2) and 8 (n = 6, n = 6) post-BDL, respectively. The cell-permeant Acridine-Orange nucleic acid binding dye was applied to assess LYM and PMN concentrations. Cell counting was performed using the Luna-FL™ Dual Fluorescence automated cell counter.

2.6. CNS immunohistochemistry (IHC)

BDL rats at 4 and 8-weeks post BDL (n = 3 per group) and SHAM operated rats at 8-weeks post-surgery (n = 3) were deeply anesthetized with 4% isoflurane (Piramal Enterprises Ltd.) and subcutaneous analgesic was injected (Temgesic (ESSEX) (0.1 mg/kg)) before transcardial perfusion with PBS, pH 7.4. Brains were removed and fixed in 4% formaldehyde PBS solution overnight at 4 °C, followed by PBS wash and 48 h cryopreservation in 30% sucrose in PBS at 4 °C. The optimum cutting temperature compound (Tissue-Tek® O.C.T. Compound) was used to embed tissue. Brains were sliced using a Leica-VT1200 S vibratome. For each rat, five different slides were analyzed (16 μm thick sagittal sections, distance between tissue sections ~250 μm), resulting in a total of 135 slides prepared.

2.6.1. CNS oxidative stress

***Oxo*-8-dG/*GPX1*:** To determine the presence of DNA oxidation (BDL 8-weeks post-surgery vs. SHAM) that can lead to DNA damage, mutations and neuronal degeneration, the mouse monoclonal Oxo-8-dG – Anti-DNA/RNA damage antibody [15A3](ab62623) (2 h at RT) at 1/200 dilution with the secondary Alexa Fluor® 488-AffiniPure Goat Anti-Mouse IgG (Jackson ImmunoResearch Europe Ltd.) (1 h at RT) at 1/200 dilution antibodies were applied. Glutathione peroxidase (intracellular antioxidant enzyme) was detected by anti-GPX1 Rabbit Polyclonal Antibody (PA5-26323, Thermofisher) at 1/100 dilution (2 h at RT) with secondary Alexa Fluor® 594-AffiniPure Goat Anti-Mouse IgG (Thermofisher) (1 h at RT) at 1/500 dilution.

SOD1/SOD2: To differentiate between Cu/ZnSOD (SOD1) and MnSOD (SOD2) activity (BDL at 4 and 8-weeks post-surgery vs. SHAM) staining with Rabbit Polyclonal SOD1 Antibody (PA5-27240, Thermofisher) (3 h at RT) at 1/100 dilution with secondary Alexa Fluor® 488-AffiniPure Goat Anti-Rabbit IgG (Thermofisher) (1 h at RT) at 1/200 dilution antibodies followed by anti-SOD2 Mouse Monoclonal Antibody (2A1, LF-MA0030,Thermofisher) at 1/500 dilution (3 h at RT) with secondary Alexa Fluor® 594-AffiniPure Rat Anti-Mouse IgG (Jackson ImmunoResearch Europe Ltd.) (1 h at RT) at 1/500 dilution antibodies were used.

2.6.2. Neuroinflammation

Interleukin-6 (IL-6): Mouse monoclonal IL-6 Antibody (10 E5, Thermofisher) (24 h at RT) at 1/200 dilution with secondary Alexa Fluor® 594-AffiniPure Rat Anti-Mouse IgG (Jackson ImmunoResearch Europe Ltd.) (1 h at RT) at 1/500 dilution antibodies were used.

IL-6 – UV–Vis spectroscopy: For quantitative evaluation of brain inflammation (BDL at 4 and 8-weeks post-surgery vs. SHAM), the IL-6 antibody-stained brain sections underwent immunofluorescence (IF) using UV–Vis spectroscopy. For fluorescence signal detection the TC5600-microscope (MEIJI-TECHNO CO.) coupled with the Ocean HDX UV-VIS spectrometer (Ocean Insight, Florida, USA) and the Lab Grade Reflection Probe R400-7-UV-VIS were used. The fluorophore signal was acquired using excitation/dichroic/emission filter sets (microscope filter cube from Chroma Technology Corporation (EM: ET610Ip, BS: ZT594rdc, EX: ET580/25)). The integration of UV–Vis spectra yielded the total IL-6 signal intensities .

2.7. Microscopy data processing

Fluorescence (for IHC) and bright field (for PMN and LYM) microscopy examination of tissue sections and blood samples was performed using a MEIJI-TECHNO TC5600 microscope. Images ware collected using the ×5, ×20 and ×50 objectives at the same resolution and processed with the INFINITY ANALYZE 7 software (Lumenera, Canada). For brain sections (Oxo-8-dG/GPX1 and SOD1/SOD2) relative quantitation of immunofluorescence using the mean fluorescence intensity (MFI) method was applied [40,41]. An average of 150 cells were examined for each group.

2.8. Statistical analysis

Data are presented as mean ± SD and % increase/decrease. For all measurements differences between the groups were assessed by *t*-Test (at each time point for SHAM vs BLD, longitudinal *ex-vivo*) or two-way ANOVA (SHAM vs BLD, longitudinal *in-vitro*) and one-way Anova with post-hoc Tukey HSD (longitudinal within the group and multiple groups comparison - SHAM vs BDL w4 vs BDL w8). For all the presented results the corresponding statistical test is additionally stated in the figure caption.

Pearson correlation analysis was performed using the mean values for each corresponding time point to test the ***correlations*** between our previously acquired longitudinal hippocampus metabolites by *in-vivo* ^{1}H-MRS (Gln and Asc) [29] and the following variables: oxidative stress markers and NH_4^+ blood values in a BDL rat model of type C HE.

Results having $p < 0.05$ were considered as significant. Significance level in all tests was attributed as follows: *$p < 0.05$, **$p < 0.01$, ***$p < 0.001$, ****$p < 0.0001$. Statistical analyses were performed using

OriginPro (OriginLab,USA).

3. Results

3.1. Chronic liver disease: biochemical measurements

The presence of chronic liver disease (CLD) was confirmed using blood biochemical measurements. In agreement with our previous work, we observed an early increase in blood NH_4^+, and plasma bilirubin and liver function tests (aspartate aminotransferase (AST/GOT) and alanine aminotransferase (ALT/GPT)) already at 2-weeks post-BDL (Fig. 1) as well as significant decrease of the blood glucose level over the course of disease development (Fig. 1), in agreement with our previous work [29,42,43]. BDL rats also presented clinical signs of chronic liver disease such as jaundice and an enlarged and nodular liver [35].

3.2. Oxidative stress in type C HE

3.2.1. EPR measurements

The release of intracellular $O_2^{\cdot-}$ was evaluated and quantified using the EPR CMH cell-permeable and non-toxic spin probe on *in-vitro* blood and *ex-vivo* hippocampus and cerebellum samples.

3.2.2. CNS OS

For SHAM operated animals, EPR revealed a significant difference in redox state between hippocampus and cerebellum (~31%, $p < 0.004$, 6-weeks post-surgery) (Fig. 2A). However, the relative OS increase in BDL rats at week 6 vs. SHAM was similar for both brain regions~42% ($p < 0.01$) (hippocampus 103.6 ± 19.1 μmol/g/min (L + R m = 0.142 ± 0.01 g) vs. 73.5 ± 16.3 μmol/g/min (L + R m = 0.175 ± 0.03 g), and cerebellum 136.8 ± 22.7 μmol/g/min (m = 0.290 ± 0.02 g) vs. 96.2 ± 27.4 μmol/g/min (m = 0.298 ± 0.02 g), respectively). In the hippocampus the longitudinal EPR measurements showed a significant increase of intracellular $O_2^{\cdot-}$ starting at 2-weeks post-BDL (+63%, $p < 0.01$) which continued to increase till week 8. Additionally, we observed a trend of intracellular $O_2^{\cdot-}$ increase in SHAM rats.

3.2.3. Systemic OS

Two weeks post-BDL and SHAM surgery a non-significant increase of blood OS was observed in both groups (Fig. 2B). At 4-weeks post-surgery the SHAM peripheral OS stabilized, reaching the value from before the SHAM surgery. In BDL rats the systemic OS continued to rise (week 4 + 26%, NS) reaching a significant increase at week 6 (+42%, $p < 0.01$) and week 8 (+60%, $p < 0.01$) post-BDL.

3.2.4. Correlations

As expected, the substantial increase of hippocampal OS in BDL rats correlated significantly with the increase in blood NH_4^+ ($p = 0.01$) and brain Gln ($p = 0.001$) as well as with the decline of brain Asc ($p = 0.003$) concentrations (Fig. 2A, below). Similarly, we observed a significant correlation between the systemic OS and blood NH_4^+ ($p = 0.005$) concentration (Fig. 2B).

3.3. NBT staining: qualitative histo-enzymatic CNS OS visualization

The purple formazan precipitate was present in both SHAM and BDL reflecting the high oxidative status of brain tissue at 8-weeks post-surgery (Fig. 2C). However, formazan precipitation was greater in the hippocampus and cerebellar granular and molecular cell layer, dentate nucleus (DN), white matter (WM) tracts of fimbria hippocampi (FH), and cerebellum of BDL rats suggesting increased $O_2^{\cdot-}$ activity in these areas (Fig. 2C).

3.3.1. Systemic OS using conventional microscopic NBT assay

Using a conventional microscopic NBT assay we were able to calculate the percentage of NBT-positive PMN and LYM cells at their basic state and after stimulation with PMA at 8-weeks post-surgery (Fig. 3A, Table 1). 23% and 1.2% of BDL PMN and LYM were classified as (+++) respectively. None of the SHAM PMN and LYM were (+++). PMA stimulation revealed a strong percentage increase of (+++) positive PMN BDL ~ 89% vs. SHAM ~56% and LYM BDL ~45% vs. SHAM ~26% cells (Fig. 3A).

3.3.2. Systemic OS using UV–Vis spectroscopy – colorimetric NBT assay

The colorimetric NBT assay was used to determine the ability of freshly isolated PMN and LYM cells to produce $O_2^{\cdot-}$ at 8-weeks post-surgery (Fig. 3B). Production of $O_2^{\cdot-}$ increased significantly in BDL rats (PMNs ~300%, $p = 0.001$, LYM ~112%, $p = 0.006$) and was related to the increase of PMN and LYM cells count as well as to the significantly higher resting oxidative burst, as determined by abovementioned microscopic NBT assay. The PMA stimulation assay revealed decreased responsiveness of BDL PMN with a relative change of 43.4% vs. non stimuated ones ($p = 0.005$), while the SHAM stimulated PMN demonstrated ~136% increase vs. non stimulated ($p = 0.001$)(Fig. 3B, Table 2). A different trend was observed for the BDL stimulated LYM, althought non significant ($p = 0.6$), an increased reactiveness was detected with a relative change of ~33%, whereas the SHAM LYM increased by only ~14% ($p = 0.5$)(Fig. 3B).

3.3.3. LYM and PMN isolation and concentration assay for systemic inflammation measurement

Leukocytosis was revealed using Acridine-Orange stained nuclei of LYM and PMN. A +215% increase in LYM ($p < 0.001$) and a +41% increase in PMN ($p < 0.01$) was observed already 2-weeks post-BDL as compared to the control SHAM rats at the same age, and continued to

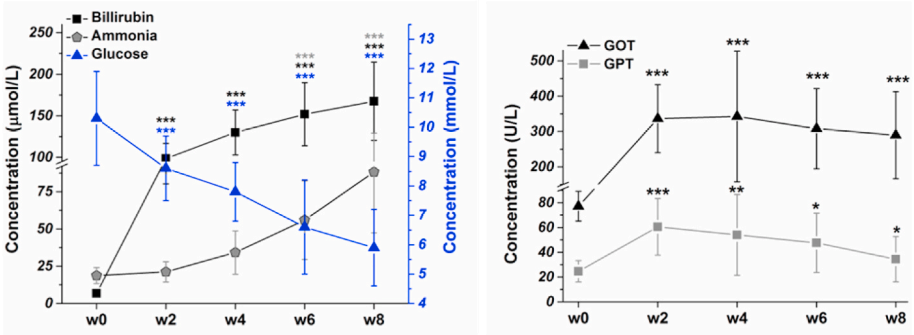

Fig. 1. Longitudinal changes in total plasma bilirubin, GOT and GPT, blood NH_4^+ and glucose induced by bile duct ligation (BDL). Bilirubin was non-measurable before BDL. Data are presented as mean ± SD and statistical significance between week 0 and weeks 2–8: *$p < 0.05$, **$p < 0.01$, ***$p < 0.001$(One-way Anova with post-hoc Tukey HSD).

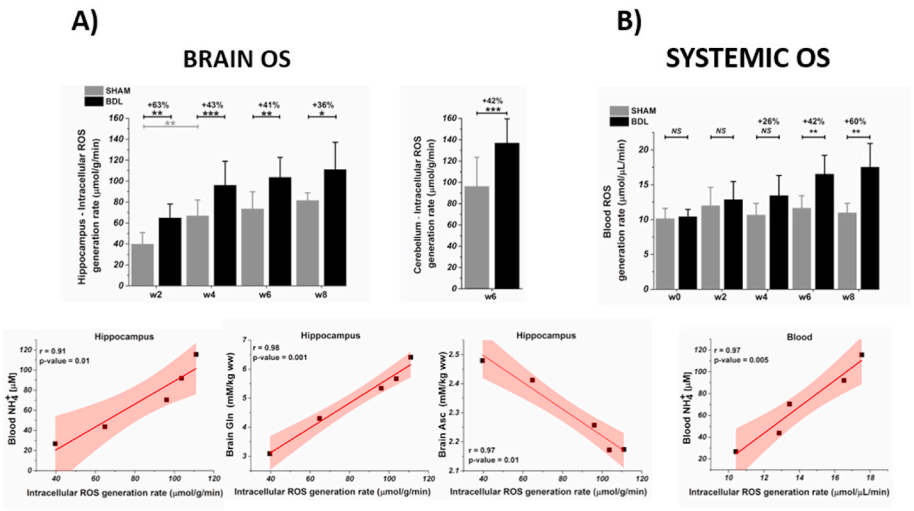

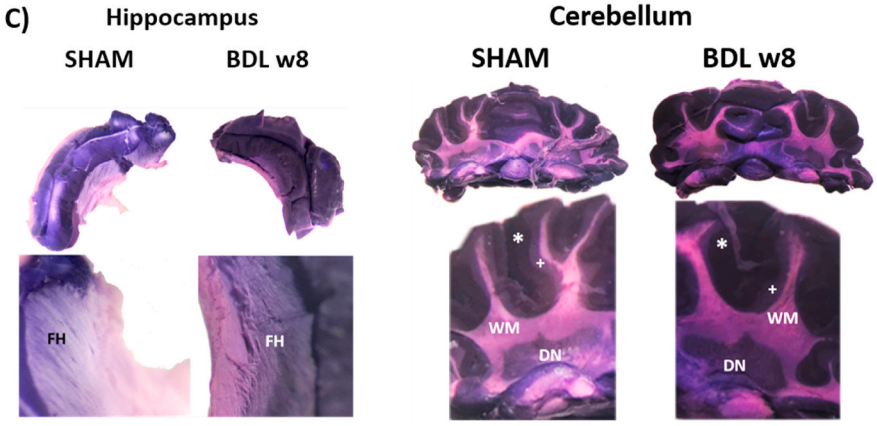

Fig. 2. Evolution of CNS OS. **A)** Longitudinal OS detection in the hippocampus from week 2 to 8-weeks post-BDL and in the cerebellum at week 6 post-BDL. The physiological pattern of age-related increase CNS redox state in SHAM rats [44]. **B)** Longitudinal evolution of systemic OS, from week 0 (before BDL) to 8-weeks post-BDL. Pearson correlations show a very strong correlation between the blood ammonia concentration and the ROS generation rate in hippocampus and blood. **C)** Photographs of representative NBT histochemical staining at week 8 post- SHAM and BDL surgery: O_2^- indirect detection. Formazan accumulation shows an increased ROS level in hippocampus and cerebellum: granular (+) and molecular (*) cell layer, dentate nucleus (DN) as well as in the white matter (WM) structures of cerebellum and hippocampus (FH – fimbria hippacampi). Data are presented as mean ± SD and statistical significance **A)** *t*-Test, **B)** Two-way Anova: *p < 0.05, **p < 0.01, ***p < 0.001.

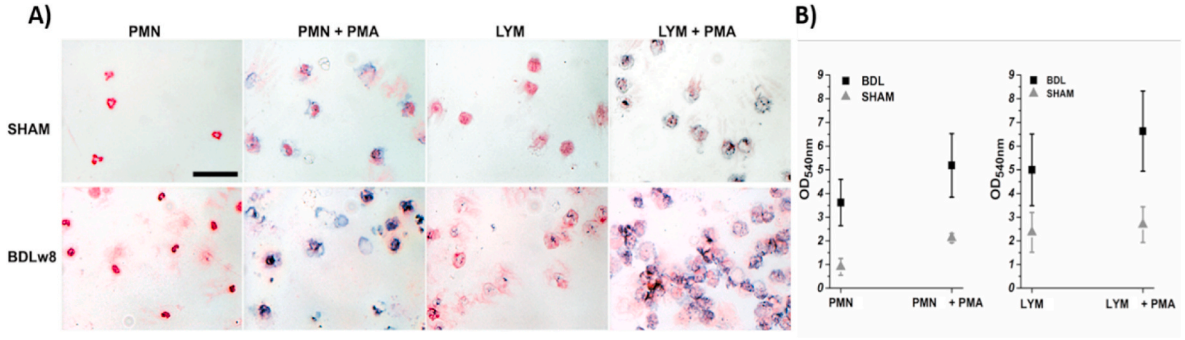

Fig. 3. A) Detection of superoxide anion (O_2^-) formation using the microscopic NBT assay at 8-weeks post-surgery. Production of O_2^- was evaluated and percentage of formazan-positive cells was determined. Cells are scored as: no detectable formazan (–), scattered formazan granules (+), intermediate density (++), and cells filled with formazan (+++) (Tab.1) **B)** Absorbance of dissolved formazan: measurements of intracellular O_2^- production using the colorimetric NBT assay at 8-weeks post-surgery in the absence and presence of stimulant at the actual PMN and LYM concentrations (Tab.2). In both assays' cells were stimulated with 400 ng/mL of PMA for 1 h at 37 °C.

Table 1
NBT staining-derived levels of ROS.

	Without stimulation				PMA stimulation			
	–	+	++	+++	–	+	++	+++
BDL PMN	10.4%	35.2%	31.4%	23%	–	–	11%	89%
SHAM PMN	2.4%	87%	10.6%	–	11.9%	5.1%	27%	56%
BDL LYM	40.5%	51.6%	6.7%	1.2%	16.2%	20.5%	18.6%	44.7%
SHAM LYM	39.1%	60.9%	–	–	7.5%	33.5%	33.1%	25.9%

Table 2
NBT colorimetric assay derived levels of ROS.

		BDL		SHAM	
		PMN $2.2 \times 10^6 \pm 0.9 \times 10^6$ cells/mL	LYM $3.2 \times 10^6 \pm 1.9 \times 10^6$ cells/mL	PMN $0.8 \times 10^5 \pm 0.3 \times 10^5$ cells/mL	LYM $1.7 \times 10^5 \pm 0.9 \times 10^5$ cells/mL
OD_{540nm}	No stimulus	3.62 ± 0.98	5 ± 1.51	0.9 ± 0.36	2.36 ± 0.22
	PMA 400 ng/mL	5.2 ± 1.5	6.63 ± 1.7	2.12 ± 0.2	2.68 ± 0.75
Relative % change		43.4	32.6	135.5	13.7

increase over the course of the study. A slightly elevated number of WBC was observed in the SHAM rats up to week 4 post SHAM surgery, compatible with surgery-induced inflammation. At 6-weeks post SHAM surgery the benign peripheral inflammation disappeared and the WBC count decreased (Fig. 4 A,C).

PMN morphology was examined on peripheral blood smears using Giemsa staining. PMN swelling, a sign of impaired phagocytosis and increased prevalence of spontaneous oxidative-burst was detected as early as 2-weeks post-BDL (+12%, $p < 0.05$)(Fig. 4 B,D). An increase of PMN count per field of view was also seen in the Giemsa stained smears (Fig. 4D). Hypersegmented neutrophils were observed already 2-weeks post-BDL surgery (Fig. 4E).

3.4. CNS immunohistochemistry

3.4.1. OS detection

We investigated the accumulation of Oxo-8-dG as a marker of DNA/RNA oxidation [45–47]. The immunofluorescent staining was of predominant cytoplasmic localization suggesting that the oxidative modifications affected mitochondrial and cytosolic nucleic acids rather than nuclear DNA. Compared to SHAM rats, the BDL rats exhibited a strong increase in Oxo-8-dG immunoreactivity in the hippocampus granular layer (stratum granulosum (SG): dentate gyrus (DG) and hilus (H),and CA1,CA2 and CA3) (Fig. 5A), and cerebellar in granular and Purkinje cells layers (Fig. 5B). Increased numbers of Oxo-8-dG positive cells was also observed in the dentate nucleus (DN) of cerebellum (Fig. 5C). Quantitative immunofluorescence of DNA oxidation revealed a significant ($p = 0.001$) increase of Oxo-8-dG accumulation in both hippocampus (granular layer + 214%, hilus +153%) and cerebellum (Purkinje cells +175%, granular cells +177% and DN +73%) (Fig. 5D).

GPX-1 showed a similar trend to Oxo-8-dG. BDL rats exhibited a significantly increased ($p = 0.001$) synthesis of GPX-1 in the cerebellar granular (+85%) and Purkinje cells layer (+92%)(Fig. 5B), and in the DN (97%)(Fig. 5C). A significant increase ($p = 0.001$) of GPX-1 synthesis was also present in the hippocampus (~95%)(Fig. 5A).

The OS driven regulation of SOD1 and SOD2 revealed an increased immunoreactivity of both antioxidants. In response to OS, SOD1 localization changed from predominantly cytoplasmic to almost prominently nuclear in all brain regions (hippocampus, cerebellum, striatum, thalamus and cortex)(Fig. 6A–E). Quantitative analysis of immunofluorescence showed significant increase of SOD1 and SOD2 ($p = 0.001$) expression in BDL rats in response to elevated endogenous and exogenous ROS (Fig. 6F). The immunofluorescence of SOD1 and SOD2 increased already at week 4 in hippocampus (granular layer: SOD1 +87%, SOD2 +13%; hilus: SOD1 +165%, SOD2 +5%), cerebellum (Pj cells: SOD1 +114%, SOD2 +42%, granular cells: SOD1 +34%, SOD2 +7%), cortex (SOD1 +100%, SOD2 +23%) and striatum (SOD1 +66%, SOD2 +44%). A similar trend was observed in the thalamus for SOD1 (+74%) while SOD2 increased significantly at week 8 post-BDL (+41%). At week 8 post-BDL SOD1 and SOD2 continued to increase in the hippocampus, cortex, striatum and thalamus, while in the cerebellum a decrease vs. week 4 was observed (Pj cells: SOD1 -9%, SOD2 -5%, granule cells: SOD1 -13.5%, SOD2 -13%).

3.4.2. Neuroinflammation

Brain sections of SHAM rats showed a weak immunofluorescence staining for IL-6. In contrast, the sections of BDL rat brains displayed a significant increase in IL-6 immunofluorescence in all brain regions (Fig. 7A–E). Immunolabeling (Fig. 7A–E) followed by UV–Vis spectroscopy of immunofluorescence revealed a statistically significant signal increase already at 4-weeks post-BDL (cerebellum +111%, hippocampus +40%, cortex +80%, thalamus +197% ($p = 0.001$) and striatum +35%: ($p = 0.01$)) corresponding to the accumulation of IL-6 (Fig. 7. A′-E′). These levels declined over time but remained higher than those of SHAM. Conversely, the hippocampus displayed a sustained increase in IL-6 signal between week 4 and week 8 post-BDL (+108%).

Cytoplasmic localization of SOD1 – arrow, translocation of SOD1 into nuclei – arrowhead. SOD2 concentration: low – arrowhead and increased – arrow. Scale bars: 250 μm for lower and 50 μm for higher magnification. Data are presented as mean ± SD and statistical significance (One-way Anova with post-hoc Tukey HSD): *$p < 0.05$, **$p < 0.01$, ***$p < 0.001$.

4. Discussion

Despite significant progress in understanding the mechanisms of type C HE, the mutual contributions of OS and inflammation in the pathophysiological cascade of type C HE are still unclear. To the best of our knowledge, this is the first study analyzing in a longitudinal fashion markers of CNS- and systemic- OS together with markers of inflammation in a rat model of type C HE by combining the experimental advantages of *ex-vivo* and *in-vitro* EPR detection of ROS, immunohistochemistry, and NBT staining. BDL rats showed increased CNS and systemic OS together with increased CNS and systemic inflammatory markers when compared to SHAM animals. Our results suggest that the increase of OS is due to enhanced formation of intra- and extra-cellular ROS rather than secondary to reduced antioxidant capacity.

In the present study, a significantly elevated $O_2^{\cdot-}$ production in the hippocampus, cerebellum, and blood of BDL rats was detected by EPR spectroscopy. This observation was confirmed by increased NBT staining, together with an overexpression of SODs, GPX-1, and Oxo-8-dG, in several brain regions of BDL rats. Importantly, the increase in systemic OS reached significance only 6-weeks post-BDL, while the increase in hippocampal OS became significant already after 2-weeks post-BDL. The elevated $O_2^{\cdot-}$ production and overexpression of SODs in brains of BDL rats may lead to an increase of H_2O_2 concentrations having a negative impact on LTP [12,48,49]. An increased activity of SOD2 enzyme ($k \sim 2 \times 10^9\, M^{-1}s^{-1},\ pH = 7.4$) could decrease EPR detection of $O_2^{\cdot-}$ concentrations through competing mechanisms with CMH spin-trap ($k \sim 10^3 \div 10^4\, M^{-1}s^{-1},\ pH = 7.4$) [33]. We can therefore hypothesize that the $O_2^{\cdot-}$ concentrations in brain tissue of BDL rats could be even higher than reported here. Additionally, a pattern of intracellular $O_2^{\cdot-}$ increase in SHAM rats was also observed, which confirms a substantial increase of OS with age [44,50].

The present results could explain our previously measured Asc decline in the hippocampus of BDL rats by *in-vivo* and longitudinal ^{1}H-MRS [29]. In the present study, we showed a strong negative correlation between the increase of $O_2^{\cdot-}$ and decrease of Asc concentrations in the brains of BDL rats. We therefore suggest that the mechanism may be through an adaptive, increased ROS scavenging in response to increased production. Asc donates a hydrogen atom to reduce toxic ROS (like $O_2^{\cdot-}$ $OH^{\cdot}$, as well as organic (RO_2) and nitrogen (NO_2) oxyradicals) and forms the ascorbyl radical and dehydroascorbic acid. However, in the presence of iron, copper and manganese ions Asc can act as a prooxidant and therefore contribute to ROS formation by enhancing ion reduction through the Fenton reaction, which may generate additional lipid,

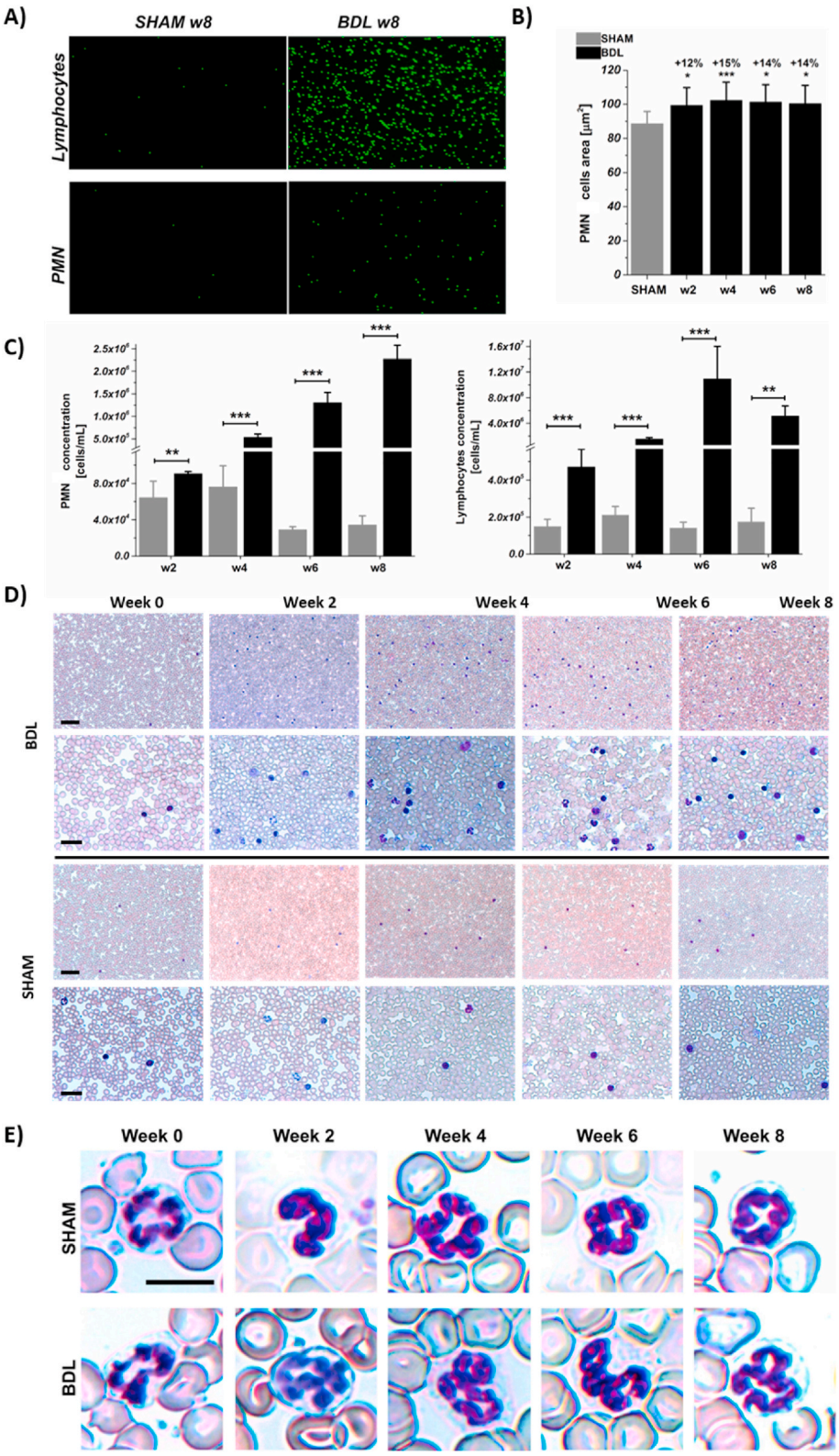

Fig. 4. **A)** Acridine-Orange stained nuclei of LYM and PMN shows significant increase of cells number in the same volume (20 μL). **B)** Giemsa staining revealed disease-induced increase of PMN cell size. **C)** Inflammatory cells count (LYM and PMN, Acridine-Orange staining). **D)** Giemsa stain: longitudinal visualization of the LYM and PMN count increase (scale bars: BDL and SHAM top rows 50 μm, BDL and SHAM bottom rows 25 μm). **E)** BDL neutrophils hypersegmentation (scale bar 10 μm). Data are presented as mean ± SD and statistical significance (*t*-Test): *p < 0.05, **p < 0.01, ***p < 0.001. (For interpretation of the references to color in this figure legend, the reader is referred to the Web version of this article.)

protein and RNA/DNA oxidation [51–53]. Furthermore, increased levels of ROS and especially interaction of the $HO^{\cdot}$ with a nucleobase, such as guanine, can result in significantly increased formation of Oxo-8-dG as shown herein in the hippocampus and cerebellum of BDL rats.

NBT staining was suggestive of increased $O_2^{\cdot-}$ production in the following anatomical regions: hippocampus, cerebellar granular and molecular cell layer, DN and WM tracts, FH structures and cerebellum. The FH white matter tracts constitute the major channel for subcortical connections of the limbic system which is associated with learning, memory and social behavior [54]. The cerebellum controls various motor activities in the brain, including the range, distance, and amplitude of voluntary muscles activity [55]. Our study revealed also that cerebellum, at its basic level, produces higher amount of ROS than hippocampus and, therefore one can speculate it to be more susceptible

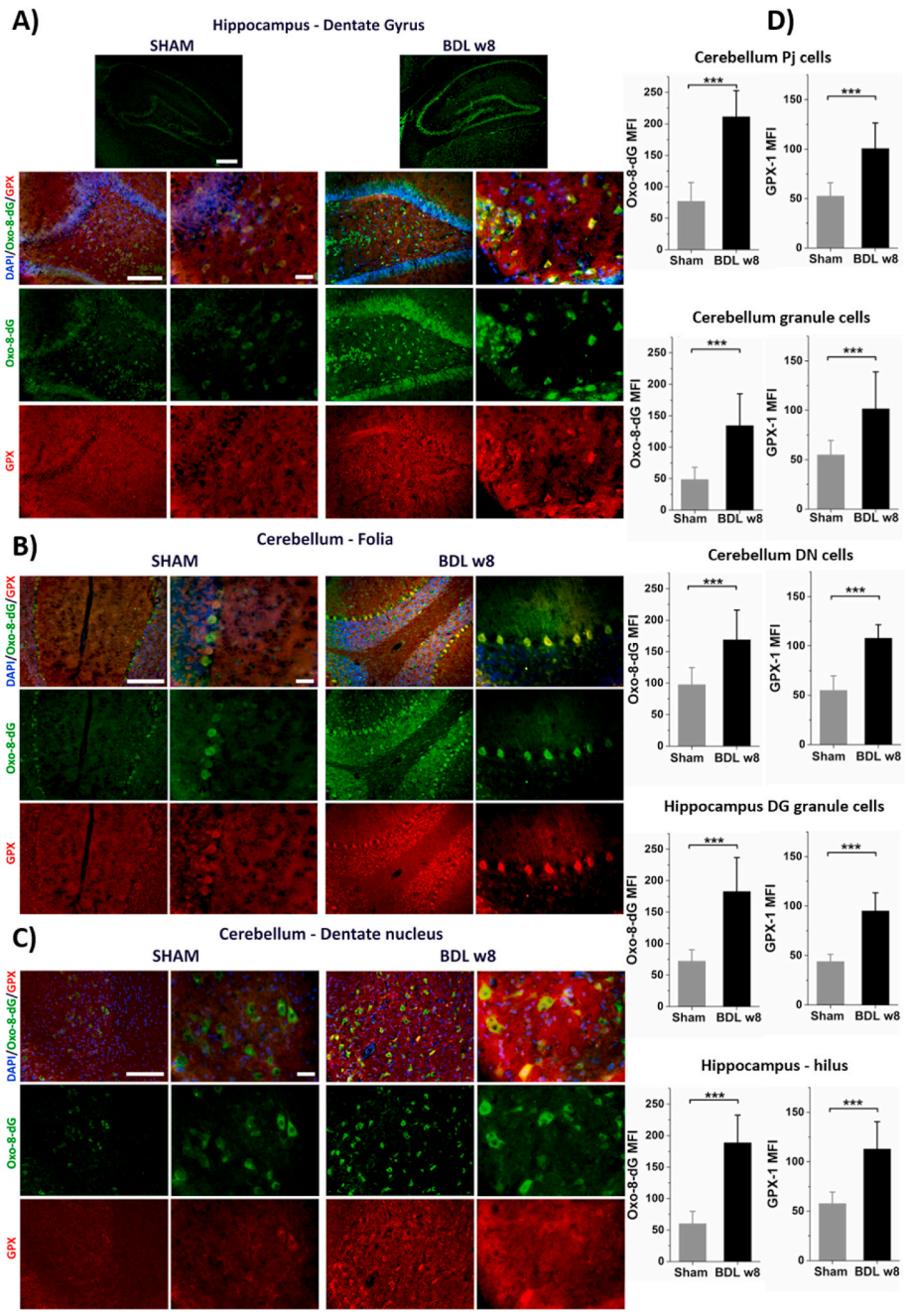

Fig. 5. Representative micrographs showing immunostaining with Oxo-8-dG (green) and GPX-1 (red) positive neurons of **A)** hippocampus (top row scale bar: 500 μm), **B)** cerebellum folia and **C)** cerebellar DN. **D)** The quantitative analyses in terms of the intensity of fluorescence of Oxo-8-dG and GPX-1 show increased levels of oxidative damage in hippocampal and cerebellar neurons of BDL rats. Scale bars: 250 μm for lower and 50 μm for higher magnification. Data are presented as mean ± SD and statistical significance (*t*-Test): *p < 0.05, **p < 0.01, ***p < 0.001. (For interpretation of the references to color in this figure legend, the reader is referred to the Web version of this article.)

to OS [56].

Type C HE is characterized by deficits in cognitive, psychiatric, and motor function [68]. Therefore, the elevated OS in cerebellum and hippocampus suggest that ROS may play an important role in brain functions disruption, and thereby provide a further link between disease progression and cognitive decline in type C HE patients.

Elevated levels of SODs were observed in the present study in response to increased endogenous and exogenous $O_2^{\cdot-}$. SOD1, being mostly located in the cytosol, has an important function in oxidative signaling and genomic DNA protection, and in presence of elevated intracellular $O_2^{\cdot-}$ levels relocates into the nucleus [57]. Our findings showed SOD1 nuclear translocation already at week 4 post-BDL as well as a significant increase in SOD1 synthesis in all brain regions. SOD2, located within the mitochondrial matrix (MM), the main source of ROS production from the electron transport chain (ETC), catalyzes $O_2^{\cdot-}$ into less reactive H_2O_2, preventing $O_2^{\cdot-}$ augmentation [58]. An upregulation of SOD2 in all brain regions is a direct evidence of increased need to eradicate ROS. Together, increased levels of $O_2^{\cdot-}$ and overexpression of SODs lead to an increased production of H_2O_2, and therefore a significant GPX-1 activity increase to detoxify H_2O_2 into water, something we observed in both hippocampus and cerebellum. These results highlight the importance of a synergistic relation between SODs and GPX-1 while dealing with increased OS.

It is well known that inflammation is associated with OS [4,59]. Under inflammatory conditions, SOD2 upregulation works as a switch to control microglial activation/inactivation [60]. We observed a significant accumulation of IL-6 in all brain regions of BDL rats already at 4-weeks post-surgery together with the presence of systemic inflammation already at 2-weeks post-BDL. IL-6 is a pleiotropic inflammatory cytokine which is expressed in both glial and neuronal cells and is implicated in the injury response of the CNS [61]. An elevated expression of IL-6 has been found in activated microglia and astrocytes, and

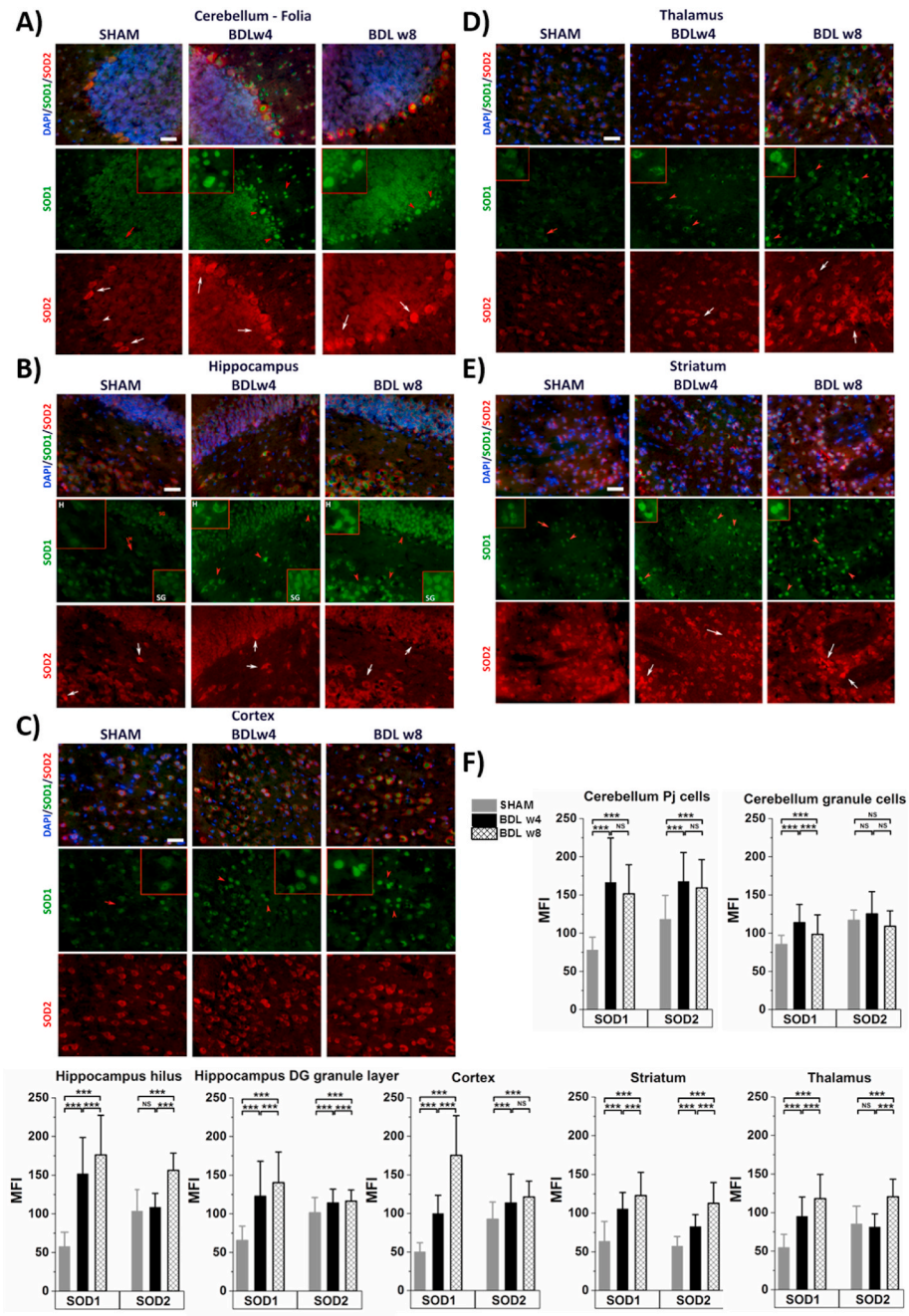

Fig. 6. Representative micrograph showing immunostaining with SOD1 (green) and SOD2 (red) positive cells. ROS-induced SOD1 translocation into nuclear localization in all brain regions as well as increased expression of both SOD1 and SOD2. **A)** cerebellum folia, **B)** hippocampus (H – hilus, SG - stratum granulosum), **C)** cortex, **D)** thalamus and **E)** striatum. **F)** The quantitative analyses in terms of the fluorescence intensity of SOD1 and SOD2 show significant increase of antioxidants expression. (For interpretation of the references to color in this figure legend, the reader is referred to the Web version of this article.)

can induce the proinflammatory cascade, as well as increased production of ROS [4,11,61–64]. In addition, IL-6 has also a complex role in regulating cognitive function. Mice with raised brain IL-6 displayed impaired cognition ability, learning loss, abnormal anxiety and abated social interactions [65,66]. Furthermore, *ex-vivo* studies of cerebral micro-vessels exposed to elevated concentrations of IL-6 have shown a significant impairment of the blood-brain barrier integrity [67]. Therefore, significant increase of IL-6 may compromise the CNS homeostasis, allow entry of neurotoxic components, and alter neuronal function.

Leukocytosis is a hallmark of systemic inflammation and an indirect sign of OS [69]. In this study, systemic inflammation was characterized by a significant increase in inflammatory cells already 2-weeks post-BDL surgery. A similar increase of leukocytes counts has been observed in HE patients, associated with an increased risk of mortality [70,71]. Ammonia and inflammation act synergistically to amplify OS in peripheral immune cells, which may explain the trend of increase in systemic OS at week 4 post-BDL surgery. It has been shown that neutrophils and lymphocytes co-exist at sites of chronic inflammation [72]. The immunological response and the oxidative metabolism of phagocytic cells increases resulting in a respiratory burst, and as a consequence enhances the release of ROS at the inflammatory site. Excess or dysregulation of production rate of ROS, may advance tissue injury and immunopathology [73,74].

The observed hyper-segmentation of neutrophils can be a hallmark of neutrophilia associated with chronic inflammation [75–79]. It has been shown that ammonium induces PMN swelling, in agreement with our findings, suggesting the presence of impaired phagocytosis and increasing prevalence of spontaneous oxidative burst [80,81]. NBT stained PMN and LYM indirectly provided information about the differential contribution of WBC in the ROS generation. In addition, NBT assay was used to determine the percentage of PMN and LYM that

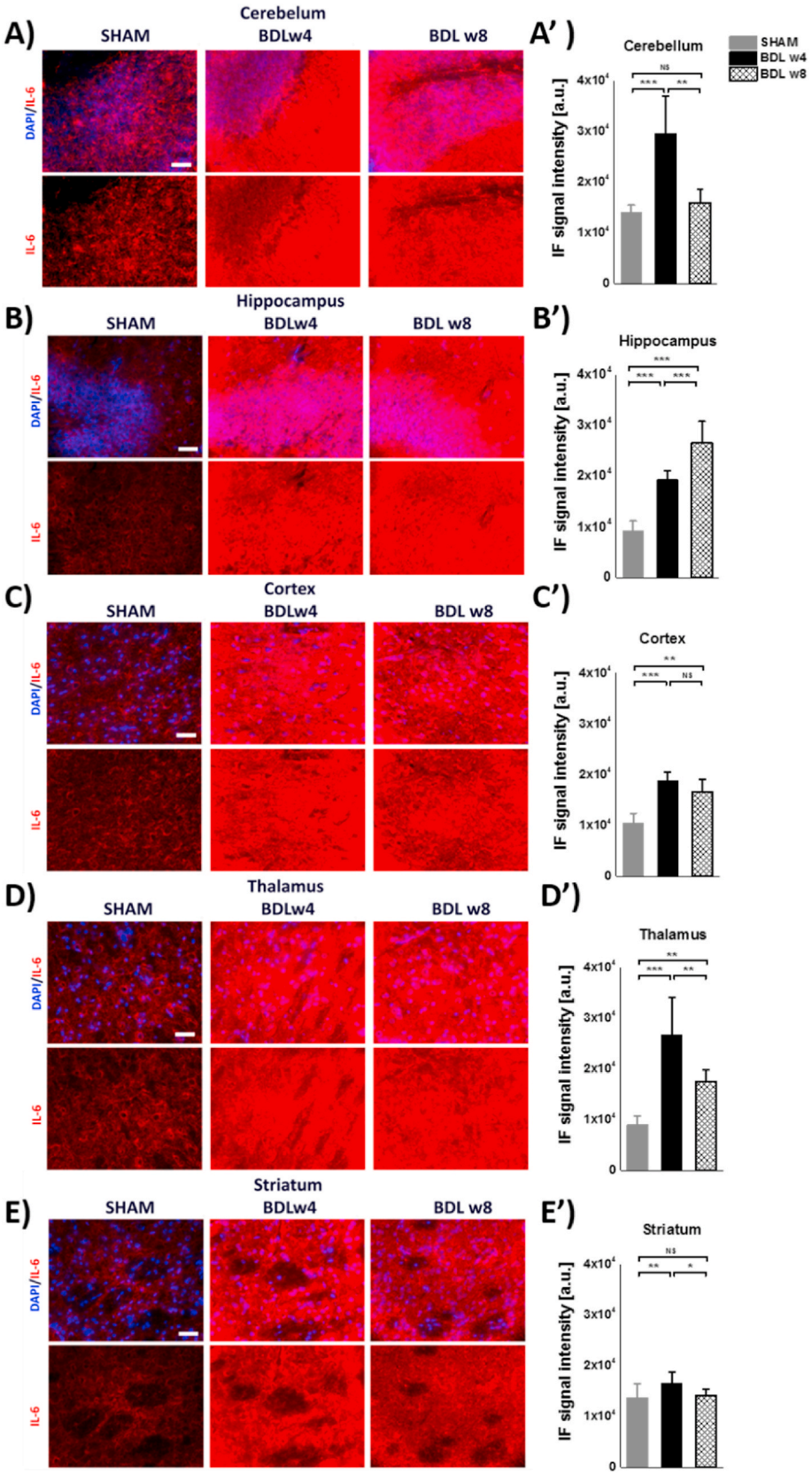

Fig. 7. Representative micrographs showing immunofluorescence staining of IL-6 (red). **A)** cerebellum folia, **B)** hippocampus, **C)** cortex, **D)** thalamus and **E)** striatum. IL-6 immunofluorescence intensity **A′-E'**. Scale bar: 50 μm. Data are presented as mean ± SD and statistical significance (One-way Anova with post-hoc Tukey HSD): *$p < 0.05$, **$p < 0.01$, ***$p < 0.001$. (For interpretation of the references to color in this figure legend, the reader is referred to the Web version of this article.)

produce ROS without and with stimulation. Our results showed that the quantity of formazan precipitants in PMN and LYM corroborated strongly with the activation state of these cells and demonstrated a significantly larger amount of $O_2^{\cdot-}$ production in BDL PMN and LYM as compared to the healthy SHAM controls. Moreover, a strong positive relation was observed between the conventional microscopic assay and the colorimetric NBT assay. PMN and LYM of BDL rats at 8-weeks post-surgery had significantly higher resting oxidative burst than the PMN and LYM of SHAM rats, suggesting their activation. Stimulation with PMA triggered an increase of oxidative burst of both BDL and SHAM WBC. However, the PMN of SHAM rats had a significantly stronger response to the stimuli compared to baseline. Stimulated LYM demonstrated a different behavior: the spontaneous oxidative burst of the BDL LYM was higher than that observed in SHAM. These results show an important role of an increased $O_2^{\cdot-}$ production by peripheral PMN and LYM on their functions and concur with the previous studies indicating that continuous neutrophil activation cause hypo-responsivity, which in turn may result in increased infection rate, organ failure and mortality [31].

5. Conclusions

Our study showed, for the first time, the concomitant and longitudinal presence of CNS- and systemic- OS together with inflammation in a rat model of type C HE. The OS results obtained by EPR were confirmed by immunohistochemistry and NBT staining. Our findings suggest that an increase in OS is due to enhanced formation of intra- and extracellular ROS rather than to reduced antioxidant performance. OS is one of the major pathways driving neurodegeneration. Therefore, CNS- and systemic- OS, together with inflammation, may strongly contribute to HE pathogenesis. Better understanding of these processes is essential to propose neuroprotective strategies that will create a new avenue of treatment of HE patients and improve the long-term cognitive outcome.

Authors' contributions

KP made substantial contributions to the conception and design of the work as well as the acquisition, analysis, and interpretation of data, and drafted the work. **DS** made substantial contributions to the acquisition and analysis of data. **AS** made substantial contributions to the acquisition of data. **DS** executed the BDL surgery and took care of the animals, executed microtomy and participated in IHC slides preparation. **SM** executed the BDL surgery and took care of the animals. **OB** contributed to the interpretation of data. **VML** contributed to the interpretation of data, provided financial support for the project, and drafted the work. **RG** provided financial support for the project. **CC** made substantial contributions to the conception of the work as well as acquisition, analysis, and interpretation of data, drafted the work and provided financial support for the project. All authors discussed the results and gave final approval to the version to be published.

Data availability

The data used to support the findings of this study are available from the corresponding author upon request.

Declaration of competing interest

The authors declare that the research was conducted in the absence of any commercial or financial relationships that could be construed as a potential conflict of interest.

Acknowledgements

Supported by CIBM, UNIL, UNIGE, HUG, CHUV, EPFL, the Leenaards and Jeantet Foundations and the SNSF project no 310030_173222 and 310030_201218.

References

[1] S. Salim, Oxidative stress and the central nervous system, J. Pharmacol. Exp. Therapeut. 360 (1) (2017) 201–205.
[2] E. Cadenas, K.J. Davies, Mitochondrial free radical generation, oxidative stress, and aging, Free Radic. Biol. Med. 29 (3–4) (2000) 222–230.
[3] M. Mittal, et al., Reactive oxygen species in inflammation and tissue injury, Antioxidants Redox Signal. 20 (7) (2014) 1126–1167.
[4] S.K. Biswas, Does the interdependence between oxidative stress and inflammation explain the antioxidant paradox? Oxid. Med. Cell. Longev. 2016 (2016) 5698931.
[5] P. Castellani, E. Balza, A. Rubartelli, Inflammation, DAMPs, tumor development, and progression: a vicious circle orchestrated by redox signaling, Antioxidants Redox Signal. 20 (7) (2014) 1086–1097.
[6] N.D. Vaziri, B. Rodriguez-Iturbe, Mechanisms of disease: oxidative stress and inflammation in the pathogenesis of hypertension, Nat. Clin. Pract. Nephrol. 2 (10) (2006) 582–593.
[7] S.I. Dikalov, Y.F. Polienko, I. Kirilyuk, Electron paramagnetic resonance measurements of reactive oxygen species by cyclic hydroxylamine spin probes, Antioxidants Redox Signal. 28 (15) (2018) 1433–1443.
[8] M. Skowrońska, J. Albrecht, Oxidative and nitrosative stress in ammonia neurotoxicity, Neurochem. Int. 62 (5) (2013) 731–737.
[9] G.H.H. Gadoth N, Oxidative Stress and Free Radical Damage in Neurology, Humana Press, 2011.
[10] E. Niedzielska, et al., Oxidative stress in neurodegenerative diseases, Mol. Neurobiol. 53 (6) (2016) 4094–4125.
[11] G. Aguilera, et al., Redox signaling, neuroinflammation, and neurodegeneration, Antioxidants Redox Signal. 28 (18) (2018) 1626–1651.
[12] L.T. Knapp, E. Klann, Role of reactive oxygen species in hippocampal long-term potentiation: contributory or inhibitory? J. Neurosci. Res. 70 (1) (2002) 1–7.
[13] C.A. Massaad, et al., Overexpression of SOD-2 reduces hippocampal superoxide and prevents memory deficits in a mouse model of Alzheimer's disease, Proc. Natl. Acad. Sci. U. S. A 106 (32) (2009) 13576–13581.
[14] A. Phaniendra, D.B. Jestadi, L. Periyasamy, Free radicals: properties, sources, targets, and their implication in various diseases, Indian J. Clin. Biochem. 30 (1) (2015) 11–26.
[15] A.J. Cooper, W.A. Pulsinelli, T.E. Duffy, Glutathione and ascorbate during ischemia and postischemic reperfusion in rat brain, J. Neurochem. 35 (5) (1980) 4.
[16] D.C. Liemburg-Apers, et al., Interactions between mitochondrial reactive oxygen species and cellular glucose metabolism, Arch. Toxicol. 89 (8) (2015) 1209–1226.
[17] V. Lachmann, et al., Precipitants of hepatic encephalopathy induce rapid astrocyte swelling in an oxidative stress dependent manner, Arch. Biochem. Biophys. 536 (2) (2013) 143–151.
[18] D. Haussinger, Low grade cerebral edema and the pathogenesis of hepatic encephalopathy in cirrhosis, Hepatology 43 (6) (2006) 1187–1190.
[19] F. Schliess, B. Görg, D. Häussinger, RNA oxidation and zinc in hepatic encephalopathy and hyperammonemia, Metab. Brain Dis. 24 (1) (2009) 119–134.
[20] B. Görg, F. Schliess, D. Häussinger, Osmotic and oxidative/nitrosative stress in ammonia toxicity and hepatic encephalopathy, Arch. Biochem. Biophys. 536 (2) (2013) 158–163.
[21] C.R. Bosoi, et al., Systemic oxidative stress is implicated in the pathogenesis of brain edema in rats with chronic liver failure, Free Radic. Biol. Med. 52 (7) (2012) 1228–1235.
[22] E. Chroni, et al., Brain oxidative stress induced by obstructive jaundice in rats, JNEN (J. Neuropathol. Exp. Neurol.) 65 (2) (2006) 193–198.
[23] B. Gorg, et al., Oxidative stress markers in the brain of patients with cirrhosis and hepatic encephalopathy, Hepatology 52 (1) (2010) 256–265.
[24] D.R. Aldridge, E.J. Tranah, D.L. Shawcross, Pathogenesis of hepatic encephalopathy: role of ammonia and systemic inflammation, J. Clin. Exp. Hepatol. 5 (Suppl 1) (2015) S7–S20.
[25] A.R. Jayakumar, K.V. Rama Rao, M.D. Norenberg, Neuroinflammation in hepatic encephalopathy: mechanistic aspects, J. Clin. Exp. Hepatol. 5 (Suppl 1) (2015) S21–S28.
[26] R. Pahwa, et al., Chronic inflammation, in: StatPearls, StatPearls Publishing Copyright © 2021, StatPearls Publishing LLC, Treasure Island (FL, 2021.
[27] J.M. Robinson, Reactive oxygen species in phagocytic leukocytes, Histochem. Cell Biol. 130 (2) (2008) 281–297.
[28] C.R. Bosoi, C.F. Rose, Oxidative stress: a systemic factor implicated in the pathogenesis of hepatic encephalopathy, Metab. Brain Dis. 28 (2) (2013) 175–178.
[29] O. Braissant, et al., Longitudinal neurometabolic changes in the hippocampus of a rat model of chronic hepatic encephalopathy, J. Hepatol. 71 (3) (2019) 505–515.
[30] F.A. Bozza, et al., Bioenergetics, mitochondrial dysfunction, and oxidative stress in the pathophysiology of septic encephalopathy, Shock 39 (7) (2013) 10–16.
[31] R.P. Mookerjee, et al., Neutrophil dysfunction in alcoholic hepatitis superimposed on cirrhosis is reversible and predicts the outcome, Hepatology 46 (3) (2007) 831–840.
[32] G. Cheng, et al., Detection of mitochondria-generated reactive oxygen species in cells using multiple probes and methods: potentials, pitfalls, and the future, J. Biol. Chem. 293 (26) (2018) 10363–10380.
[33] S.I. Dikalov, et al., EPR detection of cellular and mitochondrial superoxide using cyclic hydroxylamines, Free Radic. Res. 45 (4) (2011) 417–430.
[34] V. Rackayova, et al., H-1 and P-31 magnetic resonance spectroscopy in a rat model of chronic hepatic encephalopathy: in vivo longitudinal measurements of brain energy metabolism, Metab. Brain Dis. 31 (6) (2016) 1303–1314.

[35] S. DeMorrow, et al., 2021 ISHEN guidelines on animal models of hepatic encephalopathy, Liver Int. 41 (7) (2021) 1474–1488, https://doi.org/10.1111/liv.14911. In press.
[36] J.S. Armstrong, M. Whiteman, Measurement of reactive oxygen species in cells and mitochondria, in: Mitochondria, second ed., 2007, pp. 355–377.
[37] R.L. Baehner, L.A. Boxer, J. Davis, The biochemical basis of nitroblue tetrazolium reduction in normal human and chronic granulomatous disease polymorphonuclear leukocytes, Blood 48 (2) (1976) 309–313.
[38] H.S. Choi, et al., A quantitative nitroblue tetrazolium assay for determining intracellular superoxide anion production in phagocytic cells, J. Immunoassay Immunochem. 27 (1) (2006) 31–44.
[39] J.J. Barcia, The Giemsa stain: its history and applications, Int. J. Surg. Pathol. 15 (3) (2007) 292–296.
[40] N. Hamilton, Quantification and its applications in fluorescent microscopy imaging, Traffic 10 (8) (2009) 951–961.
[41] M. Fitzpatrick, The Open Lab Book, 2020.
[42] E. Flatt, et al., Probiotics combined with rifaximin influence the neurometabolic changes in a rat model of type C HE, Sci. Rep. 11 (1) (2021).
[43] V. Rackayova, et al., Probiotics improve the neurometabolic profile of rats with chronic cholestatic liver disease, Sci. Rep. 11 (1) (2021).
[44] B. Bellaver, et al., Hippocampal astrocyte cultures from adult and aged rats reproduce changes in glial functionality observed in the aging brain, Mol. Neurobiol. 54 (4) (2017) 2969–2985.
[45] A.F. Takashi Iida, Masatou Kawashima, Jun-ichi Nishida, Yusaku Nakabeppu, Toru Iwaki, Accumulation of 8-oxo-2' -deoxyguanosineand increased expression of hMTH1 proteinin brain tumors, Neuro Oncol. 3 (2) (2001 Apr) 73–81.
[46] K.S. Korkmaz, B. Debelec Butuner, D. Roggenbuck, Detection of 8-OHdG as a diagnostic biomarker, J. Lab. Precis. Med 3 (2018) 95, 95.
[47] M. Giorgio, et al., On the epigenetic role of guanosine oxidation, Redox Biol. 29 (2020) 101398.
[48] J.M. Auerbach, M. Segal, Peroxide modulation of slow onset potentiation in rat hippocampus, J. Neurosci. 17 (22) (1997) 8695–8701.
[49] T.C. Pellmar, G.E. Hollinden, J.M. Sarvey, Free radicals accelerate the decay of long-term potentiation in field CA1 of Guinea-pig hippocampus, Neuroscience 44 (2) (1991) 353–359.
[50] T. Ishii, et al., Endogenous reactive oxygen species cause astrocyte defects and neuronal dysfunctions in the hippocampus: a new model for aging brain, Aging Cell 16 (1) (2017) 39–51.
[51] G.R. Buettner, The pecking order of free radicals and antioxidants: lipid peroxidation, alpha-tocopherol, and ascorbate, Arch. Biochem. Biophys. 300 (2) (1993) 535–543.
[52] A. Hacışevki, An overview of ascorbic acid biochemistry, J. Faculty Pharm. 38 (3) (2009) 233–255.
[53] G.J. Halliwell B, Free Radicals in Biology and Medicine, fifth ed., Oxford University Press, New York, 2015.
[54] R.M. Per Andersen, David Amaral, Tim Bliss, John O'Keefe, The Hippocampus Book, Oxford University Press, Inc., 2007.
[55] I.O. Imosemi, The role of antioxidants in cerebellar development. A review of literature, Int. J. Morphol. 31 (1) (2013) 203–210.
[56] N.Z. Baquer, J.S. Hothersall, P. McLean, Function and regulation of the pentose phosphate pathway in brain, Curr. Top. Cell. Regul. 29 (1988) 265–289.
[57] C.K. Tsang, et al., Superoxide dismutase 1 acts as a nuclear transcription factor to regulate oxidative stress resistance, Nat. Commun. 5 (2014) 3446.
[58] J.M. Flynn, S. Melov, SOD2 in mitochondrial dysfunction and neurodegeneration, Free Radic. Biol. Med. 62 (2013) 4–12.
[59] C. Bemeur, P. Desjardins, R.F. Butterworth, Evidence for oxidative/nitrosative stress in the pathogenesis of hepatic encephalopathy, Metab. Brain Dis. 25 (1) (2010) 3–9.
[60] Y. Ishihara, et al., Dual role of superoxide dismutase 2 induced in activated microglia: oxidative stress tolerance and convergence of inflammatory responses, J. Biol. Chem. 290 (37) (2015) 22805–22817.
[61] M. Erta, A. Quintana, J. Hidalgo, Interleukin-6, a major cytokine in the central nervous system, Int. J. Biol. Sci. 8 (9) (2012) 1254–1266.
[62] W.Y. Wang, et al., Role of pro-inflammatory cytokines released from microglia in Alzheimer's disease, Ann. Transl. Med. 3 (10) (2015) 136.
[63] I. Coltart, T.H. Tranah, D.L. Shawcross, Inflammation and hepatic encephalopathy, Arch. Biochem. Biophys. 536 (2) (2013) 189–196.
[64] I. Zemtsova, et al., Microglia activation in hepatic encephalopathy in rats and humans, Hepatology 54 (1) (2011) 204–215.
[65] H. Wei, et al., Brain IL-6 elevation causes neuronal circuitry imbalances and mediates autism-like behaviors, Biochim. Biophys. Acta 1822 (6) (2012) 831–842.
[66] R. Yirmiya, I. Goshen, Immune modulation of learning, memory, neural plasticity and neurogenesis, Brain Behav. Immun. 25 (2) (2011) 181–213.
[67] S.S. Cohen, et al., Effects of interleukin-6 on the expression of tight junction proteins in isolated cerebral microvessels from yearling and adult sheep, Neuroimmunomodulation 20 (5) (2013) 264–273.
[68] T.H. Tranah, A. Paolino, D.L. Shawcross, Pathophysiological mechanisms of hepatic encephalopathy, Clin. Liver Dis. 5 (3) (2015) 59–63.
[69] J.S. Jordi Gracia-Sancho, Gastrointestinal Tissue. Oxidative Stress and Dietary Antioxidants, Academic Press, 2017.
[70] J. Vaquero, et al., Infection and the progression of hepatic encephalopathy in acute liver failure, Gastroenterology 125 (3) (2003) 755–764.
[71] N. Weiss, et al., Cerebrospinal fluid metabolomics highlights dysregulation of energy metabolism in overt hepatic encephalopathy, J. Hepatol. 65 (6) (2016) 1120–1130.
[72] I. Muller, et al., Polymorphonuclear neutrophils and T lymphocytes: strange bedfellows or brothers in arms? Trends Immunol. 30 (11) (2009) 522–530.
[73] P. Kruger, et al., Neutrophils: between host defence, immune modulation, and tissue injury, PLoS Pathog. 11 (3) (2015) e1004651.
[74] T. Narasaraju, et al., Excessive neutrophils and neutrophil extracellular traps contribute to acute lung injury of influenza pneumonitis, Am. J. Pathol. 179 (1) (2011) 199–210.
[75] C.S. Pavlov, et al., Neurological disorders in vitamin B12 deficiency, Ter. Arkh. 91 (4) (2019) 122–129.
[76] D.M. Ralapanawa, et al., B12 deficiency with neurological manifestations in the absence of anaemia, BMC Res. Notes 8 (2015) 458.
[77] S.M. Zabolotzky, D.B. Walker, Peripheral blood smears, in: A.C. Valenciano, R. L. Cowell (Eds.), Cowell and Tyler's Diagnostic Cytology and Hematology of the Dog and Cat, fifth ed., Mosby, St. Louis (MO), 2020, pp. 438–467.
[78] M. Koplay, E. Gulcan, F. Ozkan, Association between serum vitamin B12 levels and the degree of steatosis in patients with nonalcoholic fatty liver disease, J. Invest. Med. 59 (7) (2011) 1137–1140.
[79] H. Vahedi, et al., Association between serum folate levels and fatty liver disease, Clin. Nutr. Exper. 29 (2020) 30–35.
[80] D.L. Shawcross, et al., Ammonia and the neutrophil in the pathogenesis of hepatic encephalopathy in cirrhosis, Hepatology 51 (3) (2010) 1062–1069.
[81] D.L. Shawcross, et al., Ammonia impairs neutrophil phagocytic function in liver disease, Hepatology 48 (4) (2008) 1202–1212.